IEEE Photonics Journal
An IEEE Photonics Society Publication

Open Access

Design of an 845-nm GaAs Vertical-Cavity Silicon-Integrated Laser with an Intracavity Grating for Coupling to a SiN Waveguide Circuit

Volume 9, Number 4, August 2017

Sulakshna Kumari
Johan Gustavsson
Emanuel P. Haglund
Jörgen Bengtsson
Anders Larsson
Gunther Roelkens
Roel Baets

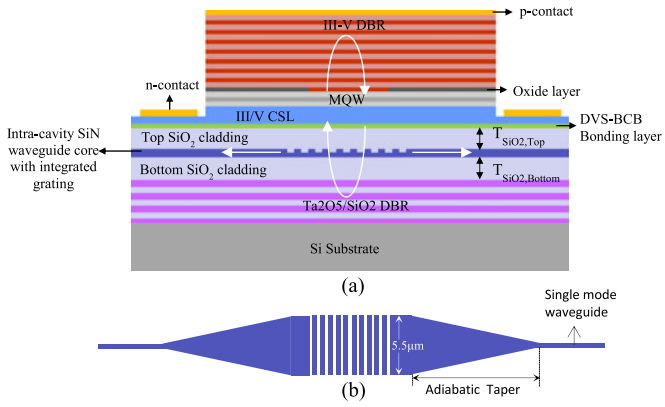

DOI: 10.1109/JPHOT.2017.2717380
1943-0655

Design of an 845-nm GaAs Vertical-Cavity Silicon-Integrated Laser with an Intracavity Grating for Coupling to a SiN Waveguide Circuit

Sulakshna Kumari,[1,2] Johan Gustavsson,[3] Emanuel P. Haglund,[3] Jörgen Bengtsson,[3] Anders Larsson,[3] Gunther Roelkens,[1,2] and Roel Baets[1,2]

[1]Photonics Research Group, imec, Ghent University, 9052 Ghent, Belgium
[2]Center for Nano- and Biophotonics, Ghent University, 9000 Ghent, Belgium
[3]Photonics Laboratory, Department of Microtechnology and Nanoscience, Chalmers University of Technology, SE-41296 Göteborg, Sweden

DOI:10.1109/JPHOT.2017.2717380

Manuscript received May 10, 2017; revised June 8, 2017; accepted June 13, 2017. Date of publication June 21, 2017; date of current version July 3, 2017. This work was supported by FP7-ERC-InSpectra Advanced Grant, European Unions Horizon 2020 research and innovation program under Grant 688519 (PIX4life), and Swedish Foundation for Strategic Research. Corresponding author: Sulakshna Kumari (e-mail: sulakshna.kumari@ugent.be).

Abstract: A short-wavelength hybrid GaAs vertical-cavity silicon-integrated laser (VCSIL) with in-plane waveguide coupling has been designed and optimized using numerical simulations. A shallow etched silicon nitride (SiN) grating is placed inside the cavity of the hybrid vertical-cavity silicon-integrated laser to both set the polarization state of the resonant optical field and to enable output coupling to a SiN waveguide with high efficiency. The numerical simulations predict that for apertures of 4 and 6-μm oxide-confined VCSILs operating at 845-nm wavelength, a slope efficiency for the light coupled to the waveguide of 0.18 and 0.22 mW/mA is achievable, respectively, while maintaining a low threshold gain of 583 and 589 cm^{-1}, respectively, for the lasing.

Index Terms: Waveguide, gratings, silicon nanophotonics, semiconductor lasers.

1. Introduction

For applications in short-wavelength optical interconnects and life sciences, photonic integrated circuits (PICs) operating in the visible (VIS) and near-infrared (NIR) with integrated sources and detectors are desired. Although there has been significant advancement in the field of silicon-on-insulator (SOI) PICs operating in the telecommunication wavelength range, this waveguide platform is not suitable for the VIS/NIR due to inter-band absorption in silicon. An alternative for this wavelength range is the use of SiN based PICs [1], [2]. They inherit the same advantages as SOI PICs in terms of fabrication, utilizing the same CMOS fabrication infrastructure, and in terms of compactness, resulting from the relatively high refractive index contrast between SiN ($n \sim 2$) and SiO_2 ($n \sim 1.5$). However, SiN does not allow for efficient light emission. This leads to the search for an attractive route of heterogeneously integrating III-V based semiconductor light sources on a SiN PIC. Several III-V-on-silicon integration techniques have been demonstrated such as the direct growth of III-V on Si [3], die-to-wafer and wafer-to-wafer bonding [4], flip-chip integration

[5]–[7] and transfer printing [8]. GaAs-based vertical-cavity surface-emitting lasers (VCSELs) are compact, possibly single mode and energy efficient sources with power conversion efficiencies that can exceed 60% [9], realized and characterized using mature wafer scale production and testing infrastructure. Therefore they would be ideally suited as light sources for these SiN waveguide circuits. The major challenge in this case is to couple the out-of-plane emission from the VCSEL efficiently into a SiN PIC.

There have been reports on coupling the VCSEL output to planar waveguides by flip chipping them onto a 45 degree mirror [10], onto a perfectly vertical grating coupler [5], or onto an angled grating coupler [6], [7]. However, these techniques suffer from not being wafer scale processes and require accurate and time-consuming alignment of individual devices. The monolithic integration of VCSELs and waveguides has also been demonstrated where the VCSEL output is coupled to on-chip planar waveguides [11]–[13]. In [11], [12], a High Contrast Grating (HCG) is used as bottom reflector and coupler for in-plane emission. However, a SiN HCG reflector requires the SiN grating to be free standing, which makes the device processing more complex [14]. In [13] the VCSEL output is coupled to monolithically grown in-plane III-V waveguide by an integrated Bragg diffraction grating placed inside the top p-DBR.

Recently, we achieved high lasing efficiency from a hybrid-cavity 845-nm wavelength VCSEL consisting of a GaAs-based half-VCSEL, i.e., active region and top DBR, bonded to a bottom dielectric distributed Bragg reflector (DBR) consisting of 20 pair of quarter-wavelength-thick Ta_2O_5/SiO_2 layers on a Si substrate [15], [16]. This integrated laser was designed for surface, i.e., out-of-plane, emission with the sole purpose of demonstrating the hybrid vertical-cavity laser integration technique. The work presented here is a continuation with a theoretical study that demonstrates that it is possible to achieve in-plane instead of out-of-plane emission from the 845-nm wavelength hybrid vertical-cavity laser basically without sacrificing efficiency, making it suitable for planar lightwave circuits. To achieve the in-plane emission and waveguide coupling, a SiN waveguide layer is introduced inside the hybrid vertical-cavity laser into which a shallow grating is etched. A gold layer is added on top of the GaAs-based DBR to prevent surface emission. Since the laser is not surface emitting, we refer to it as a vertical-cavity silicon integrated laser (VCSIL). Our approach of using an intra-cavity waveguide with integrated grating for in-plane coupling has the following advantages: (a) it allows the heterogeneous integration of GaAs-based vertical cavity light sources on a SiN waveguide circuit, (b) it selects the polarization state of the light generated by the VCSIL, (c) high efficiency waveguide coupling can be obtained and (d) as demonstrated in [15], the alignment is determined by lithography after the heterogeneous integration of the III-V material.

2. Intracavity Grating Design

The schematic of the proposed 845-nm wavelength oxide-confined VCSIL is shown in Fig. 1. The VCSIL structure consists of two distinct parts. The top half structure is a GaAs-based half-VCSEL containing a III-V top distributed Bragg reflector (DBR), a III-V active region with multiple quantum wells (MQWs), and a III-V current spreading layer (CSL). A gold layer is covering the top III-V DBR to avoid surface emission and to reduce cavity loss, and an oxide layer is positioned in the top DBR mirror pair closest to the active region to provide current confinement and optical confinement in the VCSIL. The bottom half structure consists of a weak diffraction grating etched in an intra-cavity SiN waveguide placed on top of a bottom dielectric DBR with 20 mirror pairs of Ta_2 O_5/SiO_2. A 20-nm-thick divinylsiloxane-bis-benzocyclobutene (DVS-BCB) adhesive bonding layer is used to attach the top GaAs-based half-VCSEL to the bottom dielectric DBR on Si substrate. The generated light is resonating vertically between the III-V top DBR and the grating/bottom dielectric DBR combination, and a fraction of this light energy is coupled out laterally by the grating into the SiN waveguide. Note that the output coupling is bi-directional which is useful for e.g., feeding several sensors on a bio-photonic sensing PIC. With advanced grating designs such as an asymmetric grating with etched slit [17], a binary blazed grating coupler based on an asymmetric sub-grating structure [18], or a chirped grating [19], all of the optical power can be coupled in a single direction.

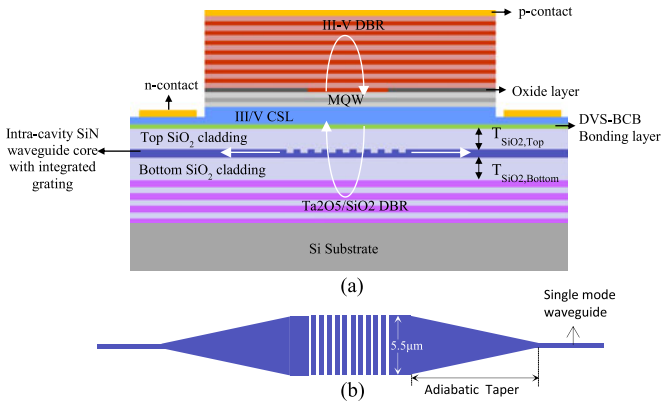

Fig. 1. (a) Schematic cross section of the 845-nm-wavelength VCSIL with in-plane out-coupling. (b) Top view of the intracavity SiN grating.

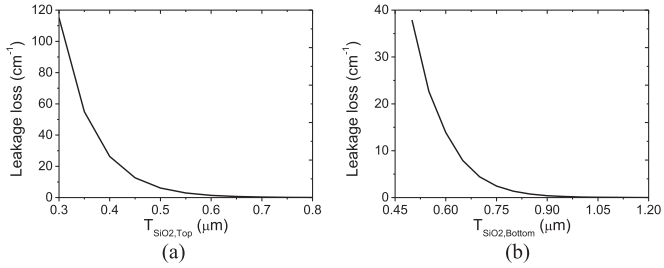

Fig. 2. (a) Oxide cladded 5.5 μm by 300 nm SiN waveguide leakage loss as a function of oxide thickness (845-nm wavelength, TE polarization). (b) Oxide cladded 500 nm by 300-nm SiN waveguide leakage loss as a function of oxide thickness (845-nm wavelength, TE polarization).

The first challenge in this design is to prevent light guided by the SiN waveguide to leak away into the high index III-V material or bottom dielectric DBR and Si substrate. Therefore, the thicknesses of the top and bottom SiO_2 cladding layers, $T_{SiO2,Top}$ respective $T_{SiO2,Bottom}$ need to be sufficiently thick to minimize this leakage loss. This leakage loss was estimated using a commercially available software FIMMWAVE, an optical mode solver from Photon Design. Fig. 2(a) shows the leakage loss into the top half high index III-V material at 845-nm wavelength as a function of $T_{SiO2,Top}$ for the fundamental TE mode in a 300-nm-thick SiN waveguide core. The SiN waveguide core has an input core width set to 5.5 μm, chosen in such a way that it matches the size of the fundamental transverse mode of the VCSIL, which in turn is determined by the diameter of the oxide aperture. An optimization of the oxide aperture diameter on the VCSIL performance is presented later. A minimum thickness of 600 nm for $T_{SiO2,Top}$ is required to minimize the leakage loss. The SiN waveguide core width is adiabatically tapered (over a length of 200 μm) from 5.5 μm at the VCSIL to 500 nm in order to make it a single mode waveguide. Moreover, the light guided by this single mode waveguide should not leak into the bottom dielectric DBR and high index Si substrate either. Fig. 2(b) shows the leakage loss into the bottom half of the structure at 845-nm wavelength as function of $T_{SiO2,Bottom}$ for the fundamental TE mode in an oxide cladded single mode SiN waveguide core (thickness 300 nm, width 500 nm). As can be seen from Fig. 2(b), a minimum thickness of 900 nm for $T_{SiO2,Bottom}$ is required to minimize the leakage loss.

Next, numerical calculations for optimizing the intra-cavity grating design were performed using Lumerical, a commercial simulator based on the finite-difference time-domain (FDTD) method. A 2D-simulation was performed on the structure shown in Fig. 3, where a Gaussian beam was launched from inside the top SiO_2 cladding layer perpendicular to the bottom half of the VCSIL cavity containing the SiN (refractive index, $n = 1.93$) waveguide core with integrated grating, the bottom SiO_2 cladding layer, and the 20 mirror pair Ta_2O_5/SiO_2 dielectric DBR. The

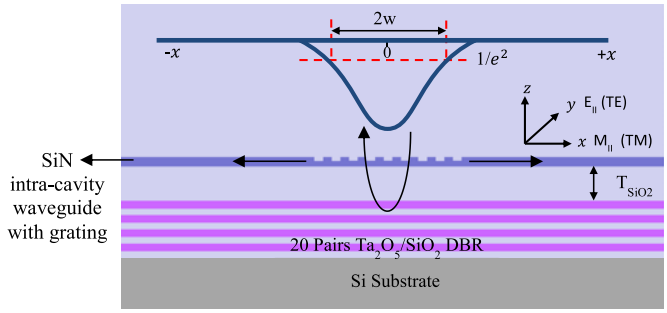

Fig. 3. Schematic cross section of the 2-D FDTD simulation setup for the intracavity grating.

quarter-wavelength-layers of Ta_2O_5 (n = 2.12) and SiO_2 (n = 1.45) have a thickness of 100 and 144 nm respectively. The Gaussian beam waist was placed 100 nm above the intra-cavity grating layer. Since the grating is placed inside the VCSIL cavity, the fraction of light energy that is coupled to the SiN waveguide in a single cavity round trip must be made small, in order to maintain a low laser threshold gain. At the same time, the in-plane coupling should be the dominant cavity loss term in the laser in order to maximize the slope efficiency for the light coupled to the SiN waveguide. This means that other cavity losses from free-carrier absorption, oxide aperture scattering, and grating diffraction are to be minimized in the VCSIL design.

The main objective of the simulation was to design a weak coupling grating at 845-nm wavelength, for light polarized parallel to the grating lines (transverse electric, TE, mode). It should provide coupling of a small fraction of light into the SiN waveguide, and at the same time it should introduce strong grating diffraction loss for light polarized perpendicular to the grating lines (transverse magnetic, TM, mode). This results in higher cavity loss for the TM mode, which can favorably be used to suppress the TM mode from lasing, i.e., set the TE polarization state for the light generated by the VCSIL.

At first, the grating period, grating groove depth, and $T_{SiO2,Bottom}$ were simultaneously optimized using a particle swarm optimization algorithm [21]. The SiN waveguide core thickness was kept fixed at 300 nm, and a grating duty cycle of 50% was chosen to offer a simpler fabrication. A Gaussian beam with wavelength span of 10 nm, from $\lambda_1 = 840$ nm to $\lambda_2 = 850$ nm, and $1/e^2$ power diameter (2w) of 5.4 μm was used for the simulation. The lateral extent of the grating, i.e., the size of grating region, was fixed to 11 grating periods, in order to match the diameter of the fundamental mode in the VCSIL. For the incident Gaussian beam, an average power reflection coefficient (R_{avg}) from grating/bottom dielectric DBR combination and power coupling coefficient (single-sided) into SiN waveguide (T_{avg}) was defined by Equation (1). In the optimization algorithm we assume that a minimum reflection coefficient, R_{min} of 0.995 was necessary to achieve a low threshold gain for the laser. When the conditions $R_{avg,TE-mode} > R_{min}$ and $(R_{avg,TE-mode} - R_{avg,TM-mode}) > 0$ were fulfilled, $T_{avg,TE-mode}$ was calculated, and the single-sided coupling efficiency defined by the ratio $T_{avg,TE-mode}/(1 - R_{avg,TE-mode})$ was used as figure of merit function for the optimization algorithm.

$$R_{avg} = \frac{\int_{\lambda_1}^{\lambda_2} R(\lambda)d\lambda}{\int_{\lambda_1}^{\lambda_2} d\lambda} \quad \text{and} \quad T_{avg} = \frac{\int_{\lambda_1}^{\lambda_2} T(\lambda)d\lambda}{\int_{\lambda_1}^{\lambda_2} d\lambda} \tag{1}$$

Simulation results for the optimized intra-cavity grating design are plotted in Fig. 4, where the grating period is 525 nm, grating groove depth is 30 nm, and $T_{SiO2,Bottom}$ is 910 nm. Fig. 4(a) shows the reflection coefficient spectrum, and Fig. 4(b) shows the single-sided coupling coefficient spectrum, for both the TE and TM polarized Gaussian beam. As can be seen from Fig. 4(b) at the VCSIL design wavelength of 845 nm, the grating operates away from the grating Bragg wavelength, and in particular for the TE-mode, residing in the tail of the coupling coefficient spectrum. For the TE-mode, this provides coupling into the SiN waveguide, while maintaining a high reflection coefficient ($> R_{min}$) for lasing. For the TM-mode, the grating operates closer to the Bragg wavelength,

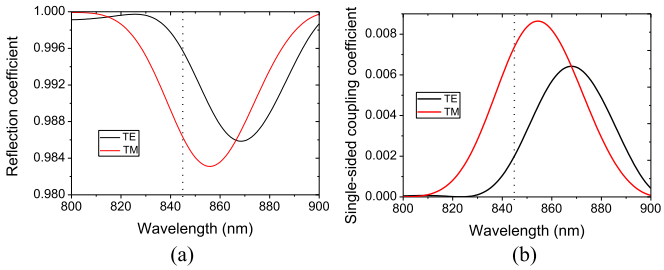

Fig. 4. (a) Reflection coefficient as a function of wavelength for TE and TM polarization. (b) Single-sided coupling coefficient as a function of wavelength for TE and TM polarization (Gaussian beam with a $1/e^2$ diameter of 5.4 μm).

resulting in a higher coupling coefficient but the reflection coefficient is much lower than what is typically needed for lasing. Thus, the intra-cavity grating provides both the functionality of in-plane output coupling and pinning the polarization state of the light generated by the VCSIL at 845 nm wavelength.

Next we assess the fabrication tolerance on the intra-cavity waveguide with integrated grating. In 1st order approximation a relative change in grating period results in an equal relative change of peak wavelength. As an effect a 10 nm increase in grating period is found to result in a 15 nm red-shift of the reflection/coupling coefficient spectrum. But the grating period can be controlled down to 1 nm using advanced patterning techniques, so this should not be an issue. Moreover, the change in peak wavelength due to change in grating duty cycle and SiN waveguide core thickness is the result of the change in the average effective index of the grating. A 20% change in grating duty cycle gives a minor 8 nm red-shift of the reflection/coupling coefficient spectrum, and a 10 nm increase in SiN waveguide core thickness results in a 3 nm red-shift in the reflection/coupling coefficient spectrum. A more critical parameter in the design is the bottom SiO_2 cladding thickness ($T_{SiO2,Bottom}$), as will be seen below. The reflection/coupling coefficient spectrum is also affected by the width of the incident Gaussian beam. The next step is therefore to optimize the diameter of the oxide aperture in the VCSIL, which will approximately correspond to the $1/e^2$ power diameter of the incident Gaussian beam. The reflection/coupling coefficient spectrum for two VCSILs with oxide aperture diameters of 4 and 6 μm were compared as function of $T_{SiO2,Bottom}$. The diameter of the fundamental transverse mode in these two VCSILs was estimated using an effective index analysis [22]. It was found that the 4 μm and 6 μm oxide aperture VCSILs correspond to a Gaussian beam with 4 and 5.4 μm $1/e^2$ power diameter respectively. Fig. 5(a)–(c) show simulation results for a Gaussian beam with a 4 μm $1/e^2$ power diameter (grating period $=$ 539 nm, grating region width $=$ 8 grating lines), and 5(d)–(f) show corresponding results for a Gaussian beam with a 5.4 μm $1/e^2$ power diameter (grating period $=$ 525 nm, grating region width $=$ 11 grating lines). Note that the double-sided coupling efficiency ($=$2*single-sided coupling efficiency) is plotted in Fig. 5(c) and (f). As can be seen in Fig. 5(a), (b), (d), and (e) the grating/bottom dielectric DBR combination reflects stronger for TE polarization than for TM polarization at 845 nm wavelength when $T_{SiO2,Bottom}$ is in the range between 880 and 940 nm, providing TE polarization selectivity in the VCSIL. By comparing Fig. 5(a) and (d), we can conclude that a Gaussian beam with 4 μm $1/e^2$ power diameter has a somewhat lower reflection coefficient than with 6 μm diameter. Since a smaller oxide aperture diameter implies a wider angular spread of the optical field inside the VCSIL, it results in a penalty in the coupling efficiency for smaller oxide apertures, comparing Fig. 5(c) and (f). Therefore, a VCSIL with large oxide aperture is preferred for optimal grating performance.

It should be noted that for achieving single transverse mode operation in a conventional 850-nm VCSEL, and most probably also for this VCSIL design, an oxide aperture diameter of 3 μm or less is required. However, such a small oxide aperture would not produce a good coupling efficiency, due to the very wide angular spread of the optical field inside the VCSIL. To obtain single transverse mode operation in a VCSIL with an oxide aperture diameter $>$3 μm, we propose the integration of a mode filter as reported in [23]. Mode filters prevent higher-order transverse modes from lasing

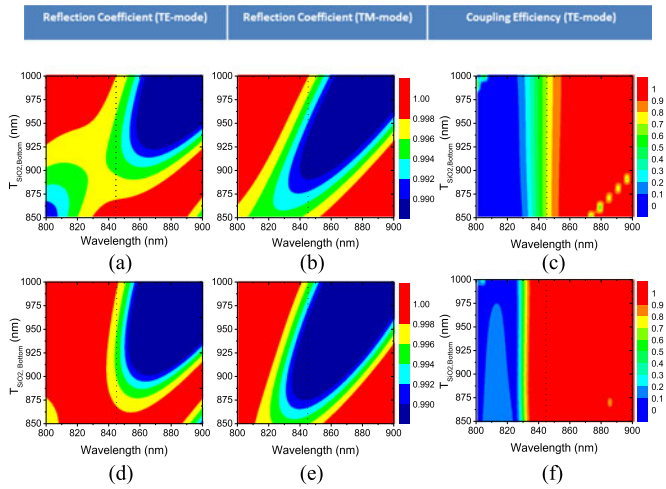

Fig. 5. Reflection coefficient as a function of $T_{SiO2,Bottom}$ for (a) TE polarization, 2w = 4 μm and grating period = 539 nm (b) TM polarization, 2w = 4 μm and period = 539 nm. (c) Double-sided coupling efficiency as a function of $T_{SiO2,Bottom}$ for TE polarization, 2w = 4 μm and period = 539 nm. Reflection coefficient as a function of $T_{SiO2,Bottom}$ for (d) TE polarization for 2w = 5.4 μm and period = 525 nm (e) TM polarization for 2w = 5.4 μm and period = 525 nm. (f) Double-sided coupling efficiency as a function of $T_{SiO2,Bottom}$ for TE polarization for 2w = 5.4 μm and period = 525 nm. Other parameters are fixed such as SiN waveguide core thickness = 300 nm, grating groove depth = 30 nm, and grating duty cycle = 50%.

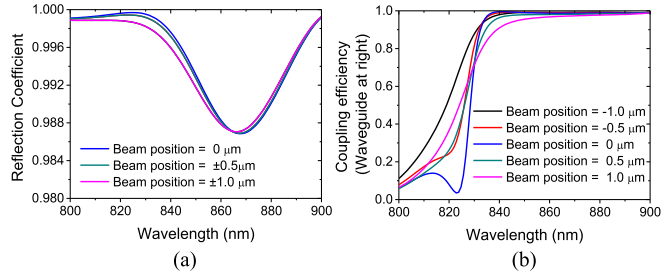

Fig. 6. (a) Reflection coefficient as a function of alignment between Gaussian beam center relative grating region center, in the direction perpendicular to the grating lines. (b) Right-hand side waveguide coupling efficiency as a function of alignment between Gaussian beam center relative to the grating region center, in the direction perpendicular to the grating lines. The grating region center is considered as the beam position = 0. Parameters of the simulations are 2w = 5.4 μm, grating period = 525 nm, SiN waveguide core thickness = 300 nm, grating groove depth = 30 nm, and grating duty cycle = 50%.

by introducing mode-selective losses in the cavity. This can be achieved by etching of a shallow surface structure in the top layer of the VCSEL structure to increase the threshold gain for higher order lateral modes [24]. With this technique, single-mode operation can be achieved for devices with oxide aperture diameters as large as 7 μm.

Finally, the dependence of the reflection coefficient and coupling efficiency on the possible lateral misalignment between the Gaussian beam (i.e., oxide aperture) and the grating region, in the direction perpendicular to the grating lines (x axis in Fig. 3) is plotted in Fig. 6. At 845 nm wavelength, a misalignment of 1 μm leads to a 0.02% drop in reflection coefficient, and a misalignment of +1 μm gives a 6% drop in coupling efficiency for the right-hand side waveguide.

3. Vertical-Cavity Silicon-Integrated Laser Design

In order to design the VCSIL as schematically shown in Fig. 1, the epitaxial design of the GaAs-based half-VCSEL demonstrated in [15], [16] is used as the top half of the structure. The bottom

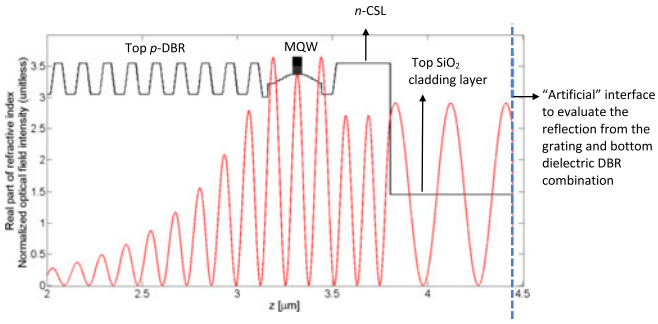

Fig. 7. Refractive index distribution (black line) and simulated resonant optical field intensity (red line) along the *z*-axis of an 845-nm-wavelength VCSIL.

half of the structure is the grating/dielectric DBR combination with the optimal parameters of the grating from Section II. To attach the top half-VCSEL to the bottom half grating/dielectric DBR combination, a 20-nm-thick adhesive DVS-BCB bonding layer is considered. In summary, the top half-VCSEL consists of a top p-doped $Al_{0.12}$ $Ga_{0.88}$ As/$Al_{0.9}$ $Ga_{0.1}$ As DBR with 23 mirror pairs, a 1-λ-thick separate confinement heterostructure (SCH) containing five 4-nm-thick $In_{0.10}$ $Ga_{0.90}$ As/$Al_{0.37}$ $Ga_{0.63}$ As QWs, and a 1-λ-thick n-doped $Al_{0.12}$ Ga0.88 As current spreading layer (CSL). A 30-nm-thick layer of $Al_{0.98}$ $Ga_{0.02}$ As is included in the DBR mirror pair closest to the SCH, for the formation of an oxide aperture via selective oxidation. Since the epitaxial structure of the GaAs-based half-VCSEL is designed for top emission, a 200-nm-thick gold layer is placed on top of the p-doped DBR to avoid surface emission from the VCSIL and to reduce cavity loss. It also provides a more uniform lateral current injection into the QWs.

The resonant optical field properties of the VCSIL cavity were analyzed using a 1D wave transfer matrix method (TMM). The grating and bottom dielectric DBR combination is replaced by an artificial interface (blue dotted line in Fig. 7) having the spectral reflection coefficient obtained from the 2D FDTD simulations in Section II. From this 1D TMM model, the resonance wavelength and optical field distribution along the optical z-axis above the grating are extracted, an example of which is shown in Fig. 7. The simulations also provide information on threshold gain and power incident on the artificial interface. From the latter we can estimate the slope efficiency for the light coupled to the SiN waveguide, via the coupling coefficient obtained from the 2D FDTD simulations in Section II. As found in Section II, the thickness of the top SiO2 cladding layer ($T_{SiO2,Top}$) needs to be around 600 nm or larger to minimize the SiN waveguide leakage loss. Also, since it is an intra-cavity layer, the thickness sets the VCSIL resonance wavelength, as can be seen in Fig. 8(a) for the two different oxide aperture diameter VCSILs. A $T_{SiO2,Top}$ thickness of 620 nm gives a resonance wavelength of 845 and 844 nm for the 4 respective 6 μm oxide aperture diameter VCSILs. A variation of 5 nm in the $T_{SiO2,Top}$ thickness shifts the resonance wavelength by approximately 0.65 nm, indicating a good fabrication tolerance. Since, DVS-BCB has a refractive index similar to SiO_2, any change in the thickness of the DVS-BCB layer translates into a similar shift in resonance wavelength as for the SiO_2 layer. As demonstrated in [15], the DVS-BCB thickness can be controlled by 10 nm with an intra-die uniformity of 5 nm. The thermal impedance in our previously demonstrated device was found to be largely unaffected by the bonding interface thickness, providing a thermal impedance of 7 K/mW [20]. This indicated that the thermal impedance was to a large extent determined by heat transport through the dielectric DBR, with the thermal impedance being 4 times larger than for ordinary GaAs-based oxide-confined VCSELs. As demonstrated in [20], the fundamental mode redshifts with temperature by 0.059 nm/K. Since the gain peak red-shifts faster with temperature than the resonance wavelength, a proper gain-to-resonance detuning is required to get optimal performance at a given temperature. The threshold gain and single-sided slope efficiency as a function of resonance wavelength for the two different oxide aperture diameter VCSILs are shown in Fig. 8(b) respective Fig. 8(c). When computing the slope efficiency an internal quantum efficiency of 85% was assumed. The penalty in coupling coefficient for a smaller oxide aperture diameter

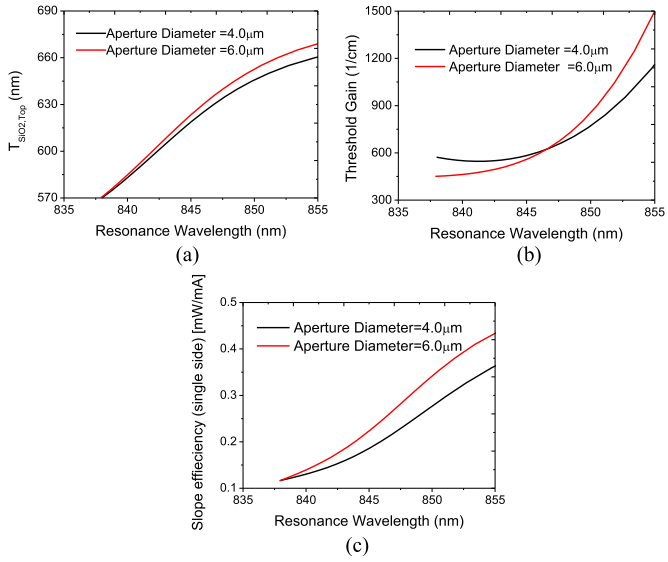

Fig. 8. (a) Top SiO_2 cladding layer thickness as a function of resonance wavelength for the VCSIL, (b) threshold gain as function of resonance wavelength, and (c) single-sided slope efficiency for light coupled into SiN waveguide as function of resonance wavelength. An internal quantum efficiency of 85% is assumed.

(as found in Section II) is reflected in Fig. 8(c) as the slope efficiency for the smaller aperture diameter is somewhat lower. Over a 10 nm resonance wavelength range from 842 to 852 nm the threshold gain is below 1000 cm^{-1}, which allows for a low threshold current, and the single-sided slope efficiency is high ($>$0.15 mW/mA), for both oxide aperture diameter VCSILs.

4. Conclusion

A VCSIL integrated with a SiN waveguide can offer a low cost, energy efficient, scalable solution for integrated laser sources in SiN photonic integrated circuits. From a numerical study, we show that it is possible to place a weak diffraction grating inside an oxide-confined 845 nm wavelength VCSIL cavity to provide a high in-plane coupling efficiency to a connected SiN waveguide while maintaining a low lasing threshold gain. The dependence of the slope efficiency (for the light coupled to the SiN waveguide) on the diameter of the oxide aperture was also investigated. An oxide aperture diameter >4 μm was found to give optimal performance. For smaller oxide aperture diameters the grating coupling coefficient is reduced by the wider angular spread of the optical field inside the VCSIL. Moreover, the intra-cavity grating is found to pin the polarization of the generated light. Thus, the presented VCSIL with an intra–cavity grating for SiN waveguide coupling is a promising design for producing an efficient laser source for various optical interconnect and sensing applications.

References

[1] A. Z. Subramanian *et al.*, "Silicon and silicon nitride photonic circuits for spectroscopic sensing on-a-chip," *Photon. Res.*, vol. 3, no. 5, pp. B47–BB59, 2015.
[2] A. Z. Subramanian *et al.*, "Low-loss single mode PECVD silicon nitride photonic wire waveguides for 532900 nm wavelength window fabricated within a CMOS pilot line," *IEEE Photon. J.*, vol. 5, no. 6, Dec. 2013, Art. no. 2202809.
[3] Z. Wang *et al.*, "Room temperature InP distributed feedback laser array directly grown on (001) silicon," *Nature Photon.*, vol. 9, pp. 837–842 2015.
[4] S. Keyvaninia, M. Muneeb, S. Stankovic, P. J. Van Veldhoven, D. Van Thourhout, and G. Roelkens,"Ultra-thin DVS-BCB adhesive bonding of IIIV wafers, dies and multiple dies to a patterned silicon-on-insulator substrate," *Opt. Mater. Exp.*, vol. 3, no. 1, pp. 35–46, 2013.
[5] Y. Wang *et al.*, "Vertical-cavity surface-emitting laser flip-chip bonding to silicon photonics chip," in *Proc. IEEE Opt. Interconnects Conf.*, 2015, pp. 122–123.

[6] K. S. Kaur *et al.*, "Flip-chip assembly of VCSELs to silicon grating couplers via laser fabricated SU8 prisms," *Opt. Exp.*, vol. 23, no. 22, pp. 28264–28270, 2015.
[7] H. Lu *et al.*, "Flip-chip integration of tilted VCSELs onto a silicon photonic integrated circuit," *Opt. Exp.*, vol. 24, no. 15, pp. 16258–16266, 2016.
[8] A. D. Groote *et al.*, "Transfer-printing-based integration of single-mode waveguide-coupled III-V-on-silicon broadband light emitters," *Opt. Exp.*, vol. 24, no. 13, pp. 13754–13762, 2016.
[9] K. Takaki *et al.*, "A recorded 62% PCE and low series and thermal resistance VCSEL with a double intra-cavity structure," in *Proc. IEEE Int. Semicond. Laser Conf.*, 2008, Post deadline paper PDP1.
[10] S. An *et al.*, "Fabrication of a 45-micro-reflector-ended polymer waveguides using one-step UV embossing technique," *Proc. SPIE*, vol. 6124, 2006, Art. no. 61241M.
[11] J. Ferrara, W. Yang, L. Zhu, P. Qiao, and C. J. Chang-Hasnain, "Heterogeneously integrated long-wavelength VCSEL using silicon high contrast grating on an SOI substrate," *Opt. Exp.*, vol. 23, no. 3, pp. 2512–2523, 2015.
[12] G. C. Park *et al.*, "Hybrid vertical-cavity laser with lateral emission into a silicon waveguide," *Laser Photon. Rev.*, vol. 9, no. 3, pp. L11–L15, 2015.
[13] D. A. Louderback, G. W. Pickrell, H. C. Lin, M. A. Fish, J. J. Hindi, and P. S. Guilfoyle, "VCSELs with monolithic coupling to internal horizontal waveguides using integrated diffraction gratings," *Electron. Lett.*, vol. 40, no. 17, pp. 1064–1065, 2004.
[14] S. Kumari *et al.*, "Integration of GaAs-based VCSEL array on SiN platform with HCG reflectors for WDM applications," *Proc. SPIE*, vol. 9372, 2015, Art. no. 93720U.
[15] E. P. Haglund *et al.*, "Silicon-integrated short-wavelength hybrid-cavity VCSEL," *Opt. Exp.*, vol. 23, no. 26, pp. 33634–33640, 2015.
[16] E. P. Haglund *et al.*, "20 Gb/s modulation of silicon-integrated short-wavelength hybrid-cavity VCSELs," *IEEE Photon. Technol. Lett.*, vol. 28, no. 8, pp. 856–859, Apr. 2016.
[17] G. Roelkens, D. Van Thourhout, and R. Baets, "High efficiency grating coupler between silicon-on-insulator waveguides and perfectly vertical optical fibers," *Opt. Lett.*, vol. 32, no. 11, pp. 1495–1497, 2007.
[18] J. Yang, Z. Zhou, H. Jia, X. Zhang, and S. Qin, "High-performance and compact binary blazed grating coupler based on an asymmetric subgrating structure and vertical coupling," *Opt. Lett.*, vol. 36, no. 14, pp. 2614–2617, 2011.
[19] X. Chen, C. Li, and H. K. Tsang, "Fabrication-tolerant waveguide chirped grating coupler for coupling to a perfectly vertical optical fiber," *Photon. Technol. Lett.*, vol. 20, no. 23, pp. 1914–1916, 2008.
[20] E. P. Haglund *et al.*, "Silicon-integrated hybrid-cavity 850-nm VCSELs by adhesive Bonding: Impact of bonding interface thickness on laser performance," *IEEE J. Sel. Topics Quantum Electron.*, vol. 23, no. 6, Nov.-Dec. 2017, Art. no. 1700109.
[21] J. Robinson and Y. Rahmat-Samii, "Particle swarm optimization in electromagnetics," *IEEE Trans. Antennas Propag.*, vol. 52, no. 2, pp. 397–407, Feb. 2004.
[22] G. R. Hadley, "Effective index model for vertical–cavity surface–emitting lasers," *Opt. Lett.*, vol. 20, no. 13, pp. 1483–1485, 1995.
[23] E. Haglund, A. Haglund, P. Westbergh, J. S. Gustavsson, B. Kgel, and A. Larsson, "25 Gbit/s transmission over 500 m multimode fibre using 850 nm VCSEL with integrated mode filter," *Electron. Lett.*, vol. 48, no. 9, pp. 517–518, 2012.
[24] .Haglund, J. S. Gustavsson, J. Vukusic, P. Modh, and A. Larsson, "Single fundamental-mode output power exceeding 6 mW from VCSELs with a shallow surface relief," *IEEE Photon. Technol. Lett.*, vol. 16, no. 2, pp. 368–370, Feb. 2004.